Supporting Information

Dissection of Fragmentation Pathways in Protonated N-Acetylhexosamines

Abhigya Mookherjee, Sanjit S. Uppal, Miklos Guttman*

Department of Medicinal Chemistry; University of Washington, Seattle, WA 98195

*Correspondence: mguttman@uw.edu

Contents:

Table S1: Accurate masses and chemical formulas for HexNAc fragment ions. *Masses were measured on a Thermo Orbitrap LTQ and calibrated using internal mass standards. The predicted chemical formulas are all within 2 ppm of the experimental masses. The chemical formulas for each ion are also consistent with the nitrogen rule [1].

measured (*m/z*)	theoretical (*m/z*)	chemical formula
204.0872	204.0872	$C_8H_{14}NO_5$
186.0766	186.0766	$C_8H_{12}NO_4$
168.0662	168.0661	$C_8H_{10}NO_3$
150.0555	150.0555	$C_8H_8NO_2$
144.0661	144.0661	$C_6H_{10}NO_3$
138.0555	138.0555	$C_7H_8NO_2$
127.0395	127.0395	$C_6H_7O_3$
126.0555	126.0555	$C_6H_8NO_2$
109.0289	109.0290	$C_6H_5O_2$
108.0449	108.0449	C_6H_6NO
99.0446	99.0446	$C_5H_7O_2$
98.0604	98.0606	C_5H_8NO
96.0451	96.0449	C_5H_6NO
84.0450	84.0449	C_4H_6NO

Table S2. Comparison of fragment ion ratios for distinguishing HexNAcs. The ratio of the intensities of *m/z* 138 to the sum of the *m/z* 138 and 144 fragments provides a reliable metric for differentiating GlcNAc and ManNAc from GalNAc. The method proposed by Halim et al [2] using the *m/z* (138 + 168) / (126 + 144) results in variations that are influenced by the anomeric state of the HexNAc.

Ion ratio	α-GlcNAc	β-GlcNAc	α-GalNAc	β-GalNAc	α-ManNAc	β-ManNAc
$\frac{138}{(138+144)}$	0.83 +/- 0.06	0.80 +/- 0.01	0.38 +/- 0.05	0.35 +/- 0.06	0.78 +/- 0.06	0.68 +/- 0.13
$\frac{(138+168)}{(126+144)}$	1.40 +/- 0.06	1.13 +/- 0.10	0.08 +/- 0.01	0.06 +/- 0.01	0.79 +/- 0.22	0.03 +/- 0.01

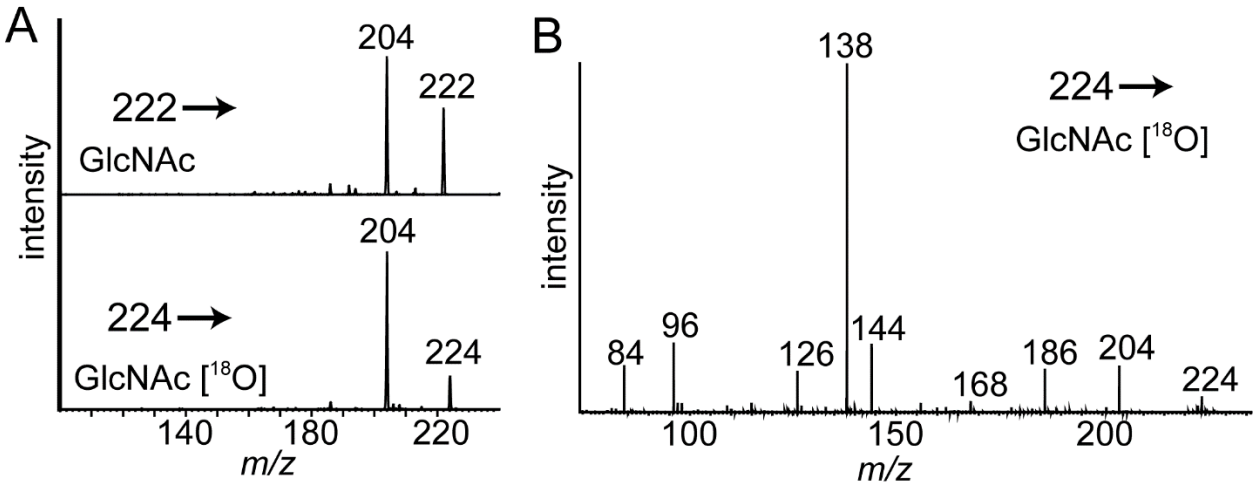

Figure S1: CID fragmentation spectrum of GlcNAc bearing an ^{18}O label at the reducing end (*m/z* 224) collected on a Thermo LTQ ion trap **(A)** or on a Waters Synapt G2-Si Q-TOF **(B)**.

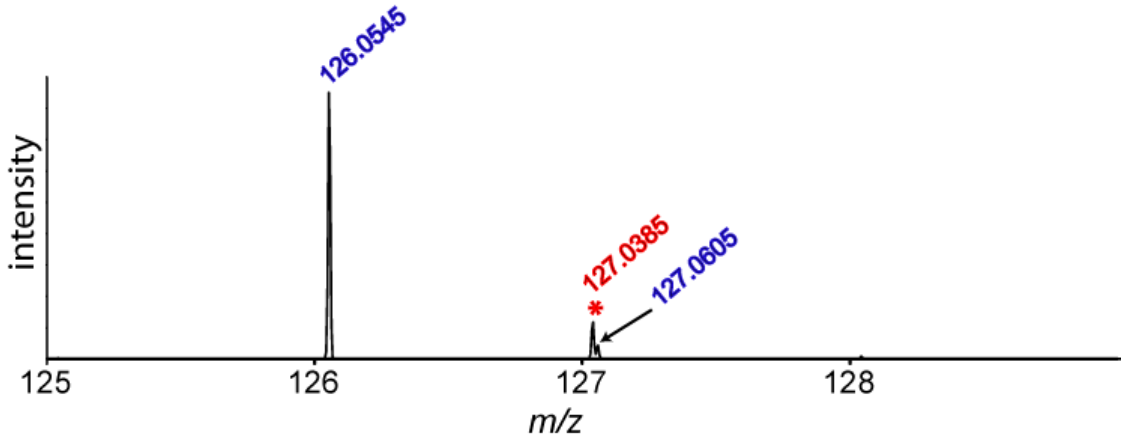

Figure S2: Detection of a unique *m/z* 127 fragment ion through high mass resolution. The abundant *m/z* 126 ion and second isotopic peak are shown in blue. The unique *m/z* 127 peak is shown in red.

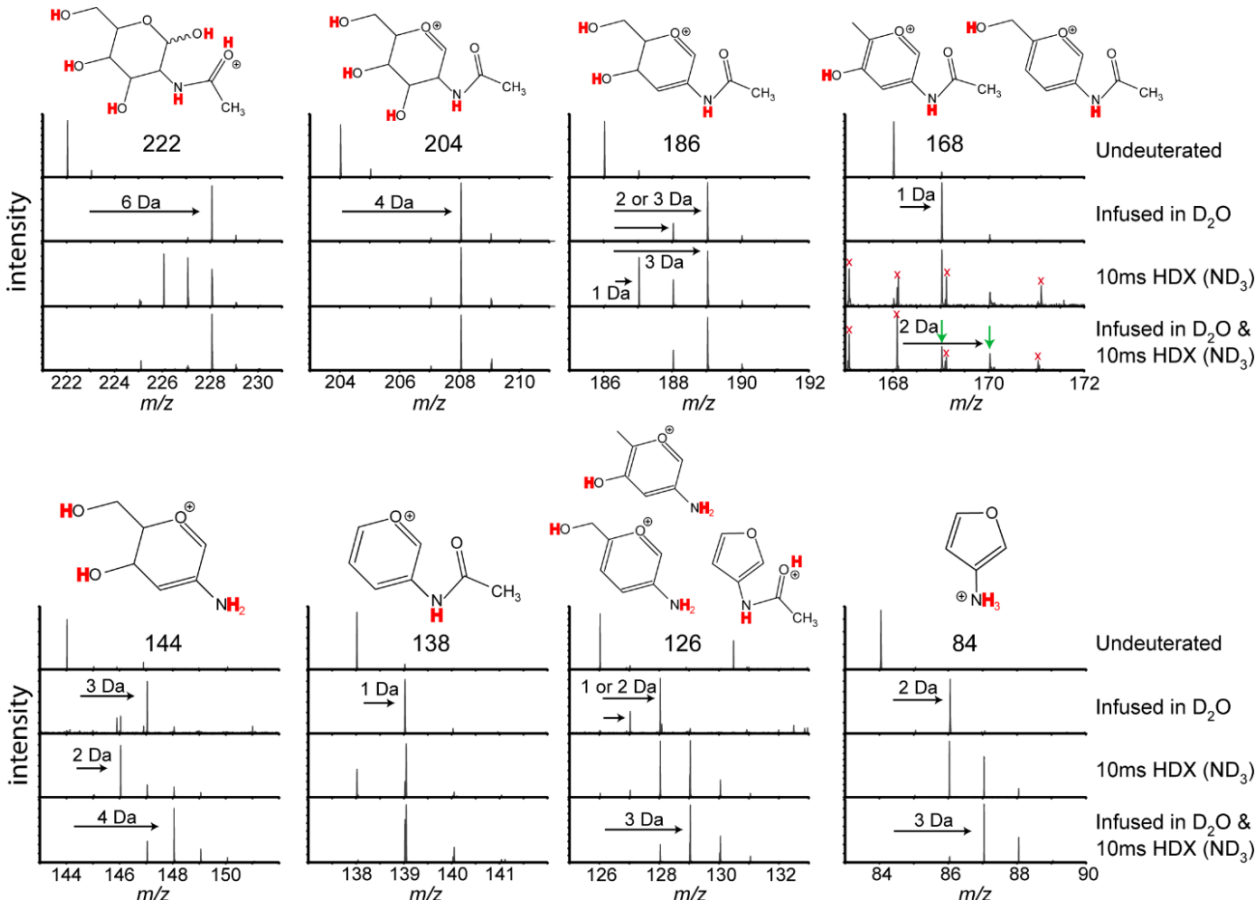

Figure S3. Solution and gas-phase deuteration of GlcNAc and its fragment ions. Spectra show the profile of each fragment as undeuterated (top), infused in D_2O (2nd panel), deuterated in the gas phase with ND_3 (3rd panel), and both infused in D_2O and subsequently deuterated with ND_3 (bottom). Exhaustive gas phase deuteration for these experiments was achieved using a ND_3 flow of 2 mL/min and an exchange time of 10 ms. Proposed structures are shown above with exchangeable/labile hydrogens shown in red. The signal for the *m/z* 168 species is largely absent in the presence of ND_3. Unrelated peaks are indicated with red x's while the actual peaks of *m/z* 168 are indicated with green arrows. GalNAc and ManNAc showed the same maximal deuterium uptake within each fragment. Additionally, this data also revealed no shift for the *m/z* 150 fragment, and the shift for the *m/z* 127* was 2 Da. Infusion in D_2O show only a 2 Da mass shift for *m/z* 84 and 144 due to the proton transfer from the methyl group to generate the protonated

amine as described previously [3]. Gas-phase HDX shows three exchangeable protons, consistent with the structure having a protonated amine. Some of the ions show a small population of increased mass (e.g. 130 in the *m/z* 126 ion spectrum), which may correspond to low levels of deuterium becoming incorporated at aromatic positions [4].

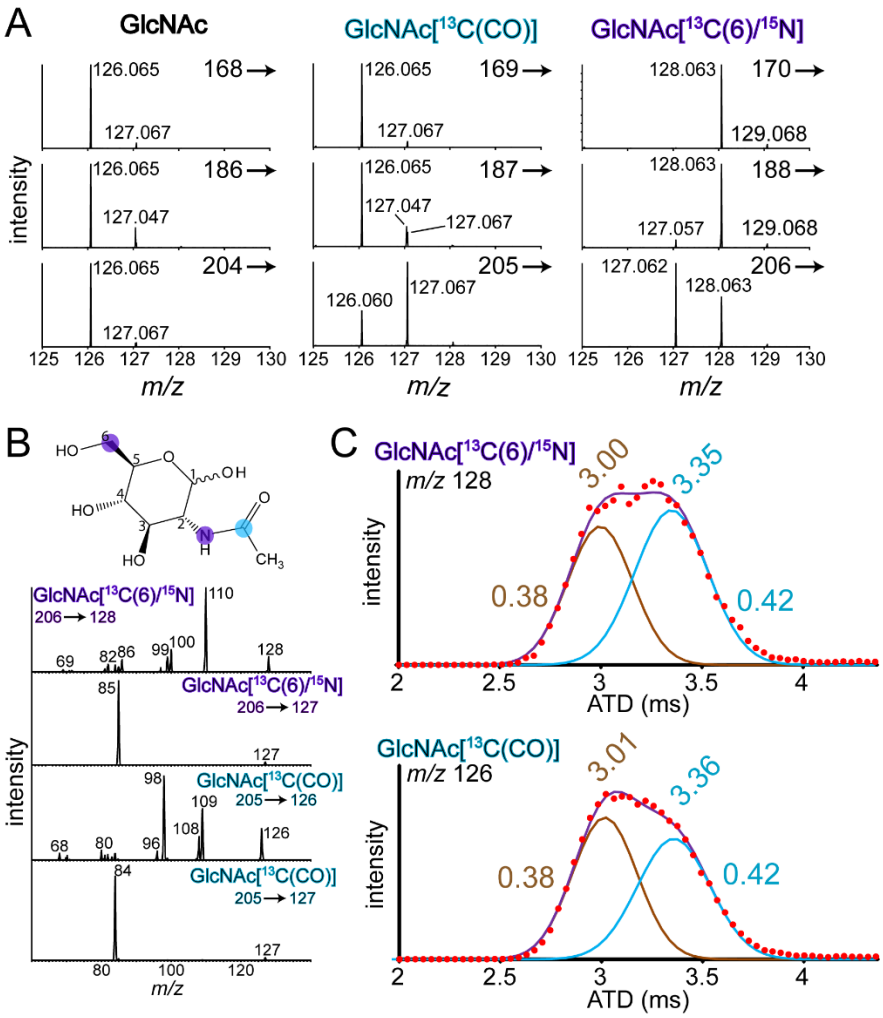

Figure S4. **A)** MS/MS spectra of various in-source fragment ions of GlcNAc, GlcNAc[^{13}C(6)/^{15}N], and GlcNAc[^{13}C(CO)], on a Waters Synapt G2-Si Q-TOF. Precursor ions are indicated within each panel. **B)** MS^{n} of isotopically labeled GlcNAc showing the difference among the *m/z* 128 and 127 species for GlcNAc[^{13}C(6)/^{15}N], and 126 and 127 peaks of GlcNAc[^{13}C(CO)]. The structure with the sites of isotopic labeling is shown above. **C)** Bimodal deconvolution of the *m/z* 128 from GlcNAc[^{13}C(6)/^{15}N] (top) and the *m/z* 126 peak from GlcNAc[^{13}C(CO)] (bottom). ATDs (in helium) are shown as red dots. The tan and blue lines show each Gaussian fit and the combination of the two Gaussians is shown in purple. Numbers above the fits indicate the center ATD and numbers to the side indicate the Gaussian width (FWHM). Label sites are shown on the left on the structure of GlcNAc.

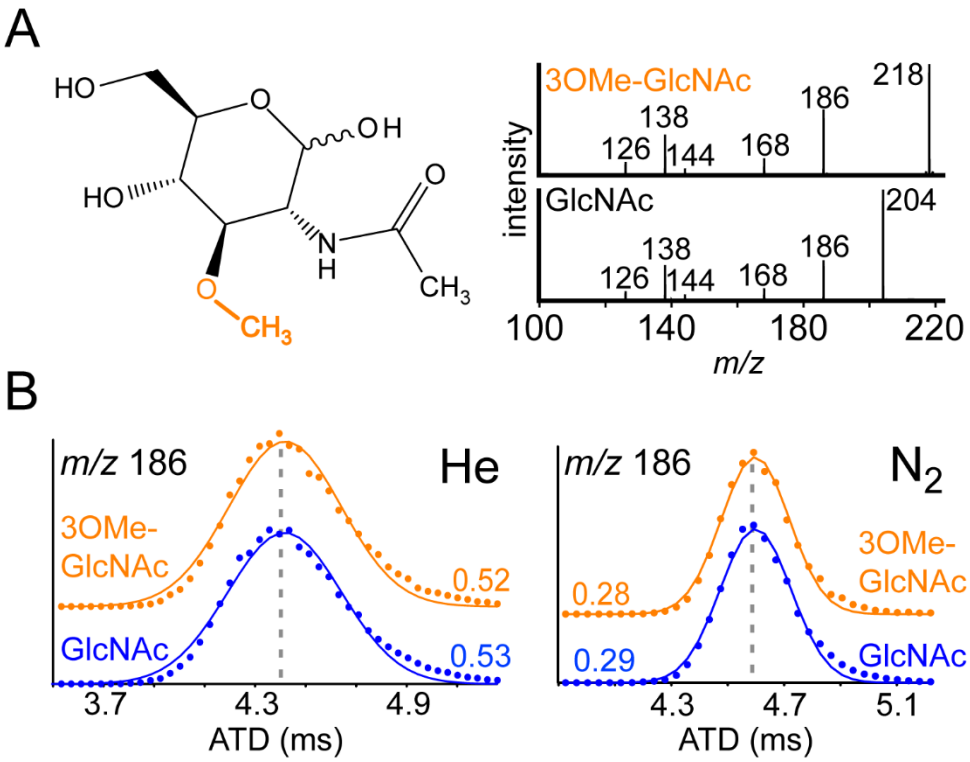

Figure S5. **A)** MS^n spectra of 3-O-methylated GlcNAc (top) vs. unlabeled GlcNAc (bottom). **B)** IM-MS analysis of unlabeled (blue) vs. 3-O-methylated GlcNAc (orange) using either helium (left) or nitrogen (right) as the drift gas. Numbers to the side indicate the Gaussian width (FWHM).

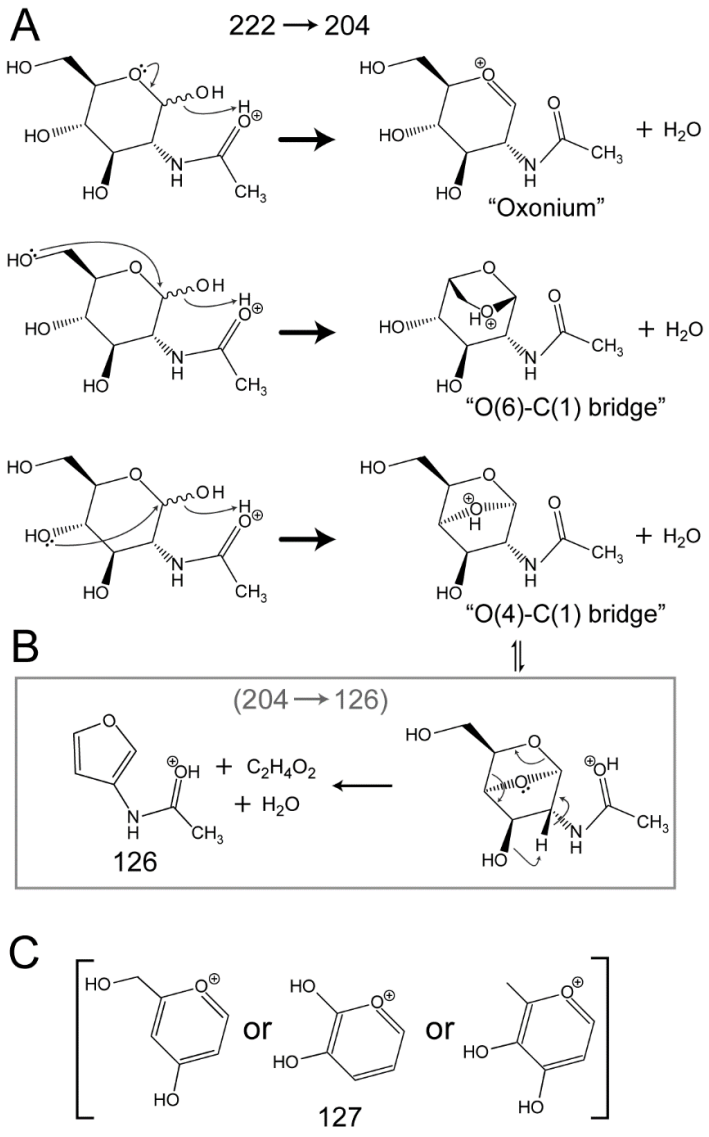

Figure S6. **A)** Proposed structures of *m/z* 204 in GlcNAc. The loss of water from the reducing end can occur through formation of a oxonium ion, or through bridging of the O(6) or O(4) with C(1). We note that this is likely only a partial list of all potential structures formed through a water loss [5, 6]. **B)** We speculate the O(4)-C(1) bridge structure can break down to form the 5-membered ring *m/z* 126 structure. **C)** Proposed structures of the minor *m/z* 127 ions.

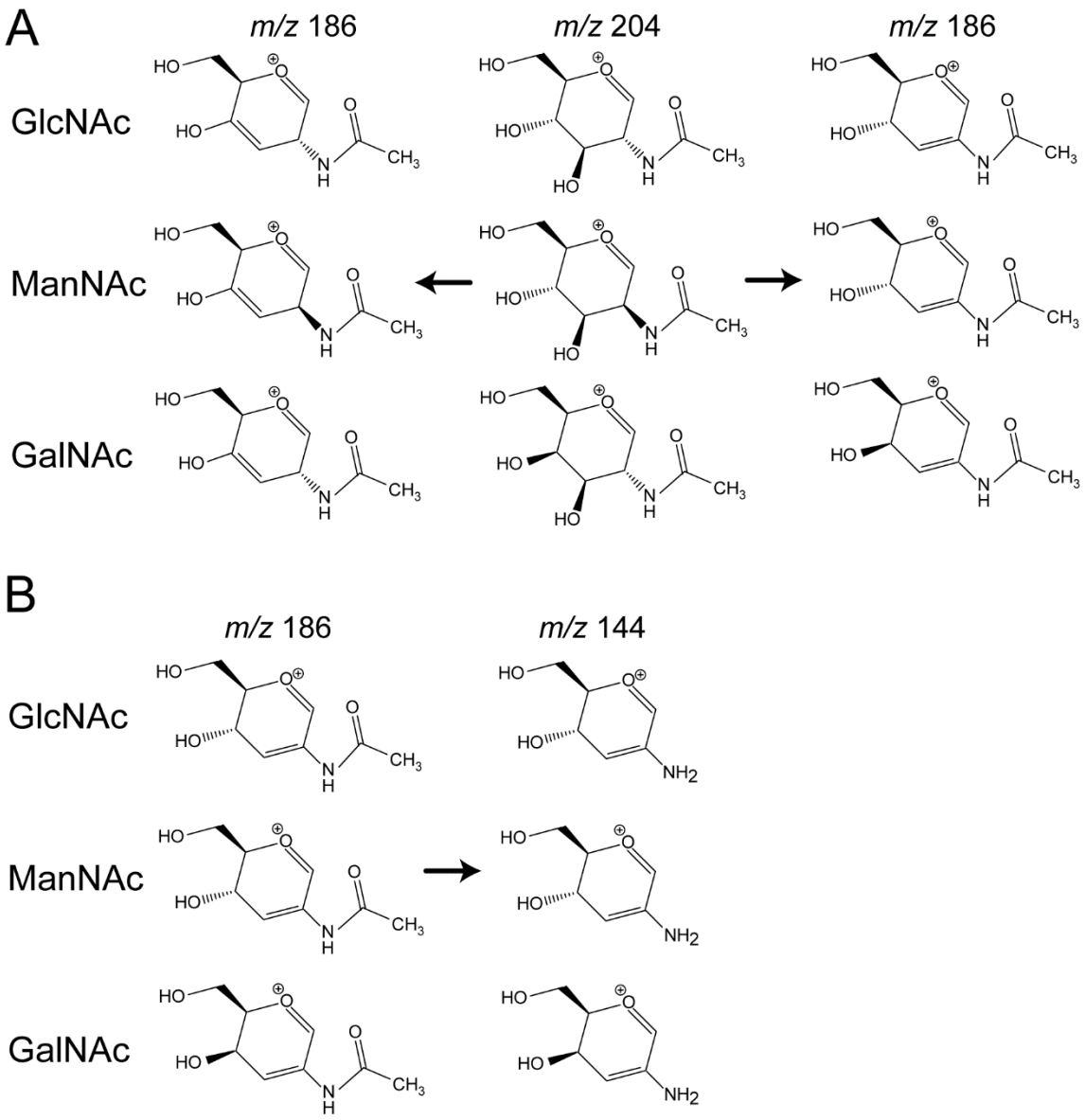

Figure S7. Diagrams of possible fragment structures of the *m/z* 186 **(A)** and *m/z* 144 **(B)** ions from GlcNAc (top), ManNAc (middle), and GalNAc (bottom).

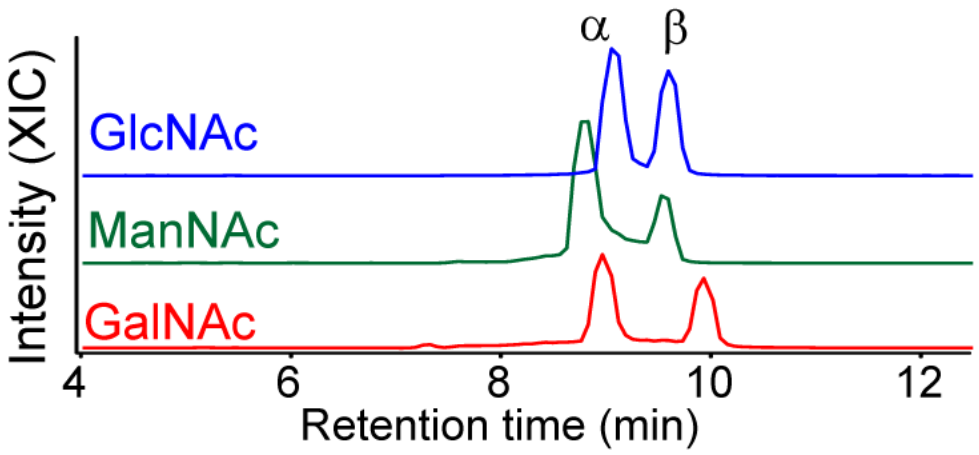

Figure S8. The α/β anomers were resolved and analyzed by MS online with hydrophilic interaction chromatography (HILIC). The extracted ion chromatogram (XIC) traces of *m/z* 204 is shown for each HexNAc. 1 μL of a 100 μM solution of each HexNAc was injected in pure water and resolved over a 2.1 x 150 mm 300 Å BEH amide column (Waters) using a gradient of 90%B to 55%B over 20 minutes (A: water with 0.1% formic acid; B: acetonitrile with 0.1% formic acid). The elution order of the anomers of these monosaccharides has been characterized previously [7] and the relative anomer intensities are consistent with previously determined equilibrium ratios [8, 9].

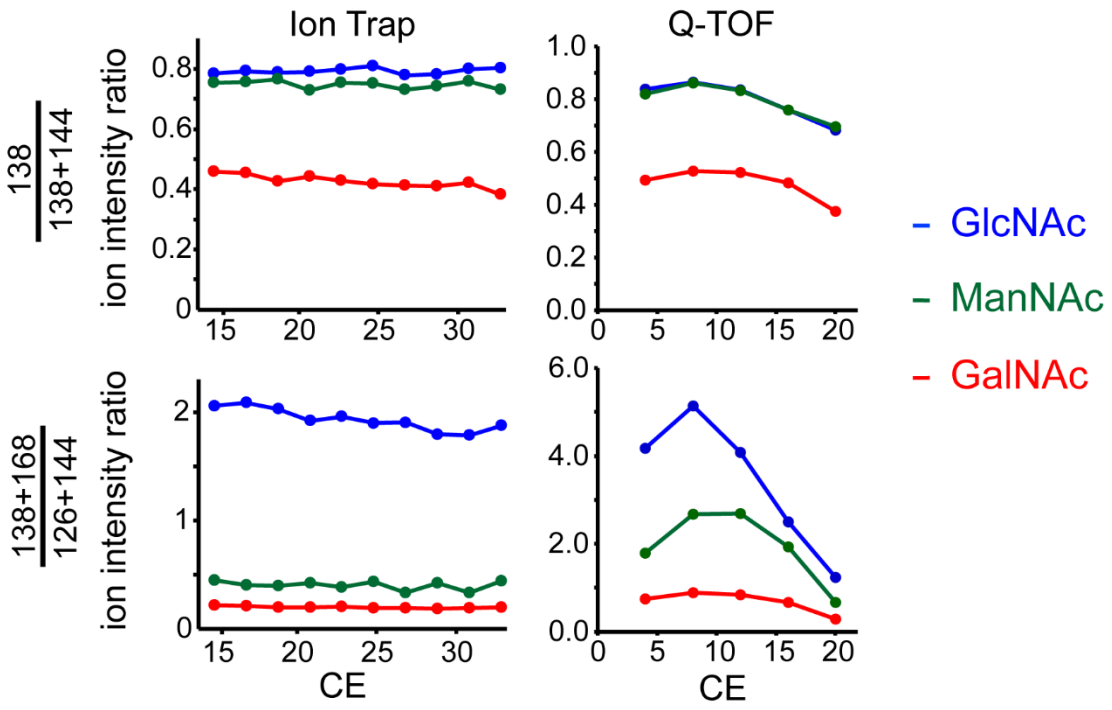

Figure S9. Collision energy dependence for the fragment ion ratios for distinguishing HexNAcs. The intensity ratio of m/z 138 / (138 + 144) [top] or m/z (138 + 168)/(126 + 144) [bottom] are shown for each HexNAc. Data were obtained on either a Thermo LTQ ion trap (left) or Waters Synapt G2-Si Q-TOF.

REFERENCES

1. F. Turecek, M. F.W., *Interpretation of mass spectra*. University Science Books: 1993; p 37-38.

2. A. Halim, U. Westerlind, C. Pett, M. Schorlemer, U. Rüetschi, G. Brinkmalm, C. Sihlbom, J. Lengqvist, G. Larson, J. Nilsson, Assignment of Saccharide Identities through Analysis of Oxonium Ion Fragmentation Profiles in LC–MS/MS of Glycopeptides. *J Proteome Res* 2014, *13*. 6024-6032, DOI: 10.1021/pr500898r.

3. J. Yu, M. Schorlemer, A. Gomez Toledo, C. Pett, C. Sihlbom, G. Larson, U. Westerlind, J. Nilsson, Distinctive MS/MS Fragmentation Pathways of Glycopeptide-Generated Oxonium Ions Provide Evidence of the Glycan Structure. *Chemistry* 2016, *22*. 1114-1124, DOI: 10.1002/chem.201503659.

4. D. R. Reed, S. R. Kass, Hydrogen–deuterium exchange at non-labile sites: a new reaction facet with broad implications for structural and dynamic determinations. *J Am Soc Mass Spectrom* 2001, *12*. 1163-1168, DOI: https://doi.org/10.1016/S1044-0305(01)00303-8.

5. B. J. Bythell, M. T. Abutokaikah, A. R. Wagoner, S. Guan, J. M. Rabus, Cationized Carbohydrate Gas-Phase Fragmentation Chemistry. *J Am Soc Mass Spectrom* 2017, *28*. 688-703, DOI: 10.1007/s13361-016-1530-x.

6. C. J. Gray, B. Schindler, L. G. Migas, M. Picmanova, A. R. Allouche, A. P. Green, S. Mandal, M. S. Motawia, R. Sanchez-Perez, N. Bjarnholt, B. L. Moller, A. M. Rijs, P. E. Barran, I. Compagnon, C. E. Eyers, S. L. Flitsch, Bottom-Up Elucidation of Glycosidic Bond Stereochemistry. *Anal Chem* 2017, *89*. 4540-4549, DOI: 10.1021/acs.analchem.6b04998.

7. D. Koga, T. Yoshioka, Y. Arakane, HPLC Analysis of Anomeric Formation and Cleavage Pattern by Chitinolytic Enzyme. *Biosci Biotechnol Biochem* 1998, *62*. 1643-1646, DOI: 10.1271/bbb.62.1643.

8. A. J. Benie, A. Blume, R. R. Schmidt, W. Reutter, S. Hinderlich, T. Peters, Characterization of ligand binding to the bifunctional key enzyme in the sialic acid biosynthesis by NMR: II. Investigation of the ManNAc kinase functionality. *J Biol Chem* 2004, *279*. 55722-55727, DOI: 10.1074/jbc.M410239200.

9. V. H. Pomin, in *NMR in Glycoscience and Glycotechnology*, ed. K. Kato, T. Peters. The Royal Society of Chemistry: London, UK, 2017, vol. 1, p 233.